



Oblique hypervelocity impacts into graphite

S Latunde-Dada

► To cite this version:

S Latunde-Dada. Oblique hypervelocity impacts into graphite. International Journal of Impact Engineering, 2011, 38 (10), pp.779. 10.1016/j.ijimpeng.2011.04.006 . hal-00842145

HAL Id: hal-00842145

<https://hal.science/hal-00842145>

Submitted on 8 Jul 2013

HAL is a multi-disciplinary open access archive for the deposit and dissemination of scientific research documents, whether they are published or not. The documents may come from teaching and research institutions in France or abroad, or from public or private research centers.

L'archive ouverte pluridisciplinaire **HAL**, est destinée au dépôt et à la diffusion de documents scientifiques de niveau recherche, publiés ou non, émanant des établissements d'enseignement et de recherche français ou étrangers, des laboratoires publics ou privés.

Accepted Manuscript

Title: Oblique hypervelocity impacts into graphite

Authors: S Latunde-Dada

PII: S0734-743X(11)00067-4

DOI: [10.1016/j.ijimpeng.2011.04.006](https://doi.org/10.1016/j.ijimpeng.2011.04.006)

Reference: IE 1996

To appear in: *International Journal of Impact Engineering*

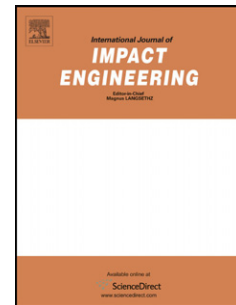
Received Date: 24 January 2011

Revised Date: 19 April 2011

Accepted Date: 19 April 2011

Please cite this article as: Latunde-Dada S. Oblique hypervelocity impacts into graphite, *International Journal of Impact Engineering* (2011), doi: 10.1016/j.ijimpeng.2011.04.006

This is a PDF file of an unedited manuscript that has been accepted for publication. As a service to our customers we are providing this early version of the manuscript. The manuscript will undergo copyediting, typesetting, and review of the resulting proof before it is published in its final form. Please note that during the production process errors may be discovered which could affect the content, and all legal disclaimers that apply to the journal pertain.



Oblique hypervelocity impacts into graphite

S Latunde-Dada

AWE Plc, Aldermaston, Reading RG7 4PR, UK

E-mail: seyi.latundedada@awe.co.uk

Abstract.

Investigations have been conducted into the morphology of craters formed by impacts of aluminium and HDPE projectiles at oblique angles to graphite target plates. The experiments were conducted with a two-stage gas gun capable of launching projectiles of differing density and strength to speeds of about 6kms^{-1} at right angles into target plates. It was found that, as the impact angle is decreased from the normal, the crater dimensions scaled as the normal component of the impact velocity as predicted by the '2/3 power law' until a critical normal velocity was reached below which the conditions for a hypervelocity impact no longer apply. In this regime, new scaling laws were derived for the crater dimensions. It was also possible to identify a fragmentation angle below which the projectile remains intact as it ricochets across the target surface.

Notation

Symbol	Explanation
p	Crater depth
d_c	Crater diameter (normal impacts)
d_t	Transverse crater diameter (oblique impacts)
d_l	Longitudinal crater diameter (oblique impacts)
d_p	Projectile diameter
$(p, d_c, d_t, d_l)^{\text{HDPE}}$	Crater dimensions for HDPE impact
$(p, d_c, d_t, d_l)^{\text{Al}}$	Crater dimensions for aluminium impact
$(p, d_c, d_t, d_l)^{\text{pred}}$	Predicted crater dimensions
$(p, d_c, d_t, d_l)^{\text{expt}}$	Experimental crater dimensions
t	Thickness of graphite block
V_c	Crater volume
v	Projectile velocity
K_p, K_d	Proportionality constants defined by equation (1)
n_p, n_d	Velocity exponents defined by equation (1)
ρ	Density
θ	Angle of impact
θ^c, θ^f	Critical and fragmentation angles of impact
$(v \sin \theta)^c, (v \sin \theta)^f$	Critical and fragmentation normal velocities
C_i	Circularity

1. Introduction

The hypervelocity impact of spheres into semi-infinite targets is a problem that has been studied extensively in the laboratory and through the use of numerical hydrocodes with in-built material models. Most of these studies have been done with ductile targets [1,2] and a few with brittle targets, examples of which can be found in [3]. Of these, most experimental studies have focused on the normal impacts where the dimensions of the craters formed have been used to characterize the damage to the target and scaling laws have been derived. These are simple power laws which, with the aid of experimental data, relate the crater dimensions to the governing parameters of the cratering process. In addition, there have also been a variety of studies into oblique planetary impacts two of which are reported in [4,5]

In [6], the 2/3 power law, which has been verified for a variety of ductile materials, was derived by correlating the projectile energy to the volume of the crater formed. This states that the crater depth p and diameter d_c normalized to the projectile diameter d_p scale as the impact velocity v raised to the power of 2/3.

$$\begin{aligned}\frac{p}{d_p} &= K_p v^{n_p} = K_p v^{\frac{2}{3}}, \\ \frac{d_c}{d_p} &= K_d v^{n_d} = K_d v^{\frac{2}{3}},\end{aligned}\tag{1}$$

where n_p , n_d are velocity exponents and K_p , K_d are proportionality constants. In [6], the morphology of craters formed in brittle targets such as graphite was discussed. There, it was pointed out that during the later stages of a hypervelocity impact, the strength of a brittle target plays a significant role in the cratering process. This causes sub-surface fractures to occur which lead to spallation of the surface around the initial crater resulting in shallower craters than those obtained in ductile targets. However, despite this difference, it was shown in [6] that the 2/3 power law should still hold for brittle craters. Table 1 shows the values obtained for the velocity exponents n_p and n_d and the proportionality constants K_p and K_d .

Table 1. Correlation parameters for crater depth with impact velocity.

Projectile Material	ρ/gcm^{-3}	n_p	K_p	n_d	K_d
HDPE	0.969	0.6972	0.7837	0.718	1.9498
Aluminium	2.71	0.6059	1.0754	0.6655	3.1472

It can be seen that for both projectiles, the 2/3 law is obeyed approximately. In [6], by assuming a power law variation for the velocity exponents n_p and n_d and the constants K_p and K_d with density ρ , the following correlations were determined:

$$\begin{aligned}\frac{p}{d_p} &= 0.791 \rho^{0.2339} v^{0.6936} \rho^{-0.1146}; \rho < 3.69 \text{ gcm}^{-3}, \\ \frac{d_c}{d_p} &= 2.02 \rho^{0.4061} v^{0.6974} \rho^{-0.0758}; \rho < 3.69 \text{ gcm}^{-3}.\end{aligned}\tag{2}$$

This was used to predict, with success, the crater dimensions for isolated experiments that were not included in the fits.

In this article, experimental data from oblique impacts into graphite will be similarly analysed and used to develop the scaling laws for oblique impacts.

This paper is laid out as follows. In Section 2, the experimental programme and procedures are described. In Section 3, the phenomena accompanying oblique impacts are discussed and the data obtained from oblique impacts are presented and analysed in Section 4. In Section 5, conclusions are drawn and recommendations for future work are made in Section 6.

2. Materials and methods

The experiments were conducted with a two-stage light gas gun which is used to accelerate small spherical projectiles to hypervelocity speeds (approximately $1\text{--}7\text{kms}^{-1}$) into target plates. It operates by the ignition of a propellant charge to force a piston forward into a breech filled with hydrogen gas at pressures of 200–500psi. This pressure rapidly increases until a bursting disc ‘petals’ and the sabot containing the projectile is launched forward. The sabot is stripped either by a metal obstruction or gas pressure and the speed of the projectile is measured by lasers just prior to impact into the target plate.

The spherical projectile materials used include HDPE and Aluminium-2024T351 with diameters ranging from 1–4.76mm. The thickness of the blocks used varied from 50mm to 100mm. The target blocks were made of commercial graphite (Graphite 25) which is a brittle and porous material with a porous density of 1.83gcm^{-3} and a compact density of 2.13gcm^{-3} . More properties are given in Table 2.

Table 2. Graphite 25 material properties

Main Characteristic	Value
Average grain size/ μm	5
Thermal conductivity/WmK	69
Coefficient of thermal conductivity/ $\mu\text{m}/\text{m}^\circ\text{C}$	5.7
Flexural strength/MPa	75
Compressive strength/MPa	170
Young's Modulus/GPa	13
Shear Modulus/GPa	4.8
Shore Hardness	79

The primary method of quantitative damage comparison between each impact is the measurement of the crater depth, diameter and volume using a laser scanner which generates profiles of the craters. Due to the irregular nature of the craters, the depth and diameter are taken in two perpendicular planes and the averages of each are found. The crater volumes are also calculated. The experimental data obtained from these experiments are tabulated in appendix A.

3. Oblique Impact Phenomena

Studies into oblique impacts [7] have shown that as the impact angle θ is decreased from the normal ($\theta = 90^\circ$) to the target surface ($\theta = 0^\circ$), the cross-section of the craters stays circular until a critical angle θ^c is reached at which the crater edge becomes elliptical. This phenomenon arises because, at angles below θ^c , the intensity of the longitudinal shock wave excited in the target is insufficient to deform the target and projectile and hence the crater dimensions are determined by the plastic flow of materials in the colliding bodies and the tangential velocity of the projectile. Since the normal component of the impact velocity excites the longitudinal shock wave, it would be prudent to refer to a critical normal velocity ($v\sin\theta^c$) rather than a critical angle θ^c . However, in this report, depending on their suitability, both terms will be used interchangeably.

Below the critical normal velocity, there are now three crater dimensions to be defined: its depth p and its diameters transverse to d_t and along d_l , the projected direction of the projectile on the target surface. These are illustrated in figure 1.

The projectile ricochets (rebounds) from its point of impact (either intact or in fragments) continuing on a slightly altered trajectory with speeds comparable to its initial impact speed [4,5]. This either elongates the crater or creates additional secondary craters downrange of the initial primary crater. The projectile material can rebound either intact or in fragments depending on whether the initial shock wave on impact has the time to travel through the projectile to fragment it before it has completely impacted the target material. This implies there is a fragmentation angle $\theta^f < \theta^c$ below which the projectile rebounds intact and above

which the projectile fragments. The degree of fragmentation is expected to be greatest at θ^c with bigger and fewer fragments as θ is decreased from θ^c to θ^f . It is also expected that θ^f decreases with increasing impact velocity. This is illustrated in the v - θ plot in figure 2.

For impact angles above θ^c , several studies [3, 7, 8, 9, 10] have revealed that both p and d_t (d_c) scale with the normal component of the impact velocity $v \sin \theta$ to the power of $2/3$ just as for normal impacts. Below the critical angle, since the projectile does not fully impact the target, p and d_c are expected to differ from the values predicted by the power laws [5, 11]. Not many studies have been carried out into the correlation with d_t , but this might be expected to vary with the longitudinal component of the velocity, $v \cos \theta$.

4. Results and Discussion

4.1 The critical normal velocity ($v \sin \theta$)^c

The experimental data from the oblique impacts of HDPE and aluminium projectiles into graphite is reported in tables A1 and A2 of appendix A. The data is analyzed in the following subsections.

4.1.1 Circularity.

For both projectile types, the circularity C_i defined as

$$C_i = \frac{d_t}{d_l}, \quad (3)$$

is plotted against the impact angle θ in figure 3 and the normal component of the impact velocity $v \sin \theta$ in figure 4.

In figure 3, the thick lines trace the average values of C_i at each impact angle. Note that, as recorded in table A1, there are no data points for HDPE at 5° because no primary craters were observed.

For aluminium projectiles, it appears that the circularity rises from values less than 1 as the impact angle is increased before it levels out at around $\theta = 30^\circ$. This is as expected with $d_l > d_t$ at angles below 30° indicating a ricocheting trajectory as the projectile scours the target surface in the direction of the trajectory path.

For HDPE projectiles, however, the opposite appears to be the case with the circularity decreasing from a value greater than 1, to a value of about 1 at 22.5° , before rising and leveling out at $\theta = 30^\circ$. The initial decrease, which indicates that for impact angles less than 22.5° the craters become elongated transverse to the trajectory path, is unusual and has also been reported in [7]. This may be because the HDPE projectile, being less dense than graphite, has minimal contact with the target at these angles and ricochets off the surface without causing much scouring in the longitudinal direction. It may be concluded however that the critical angle θ^c for both aluminium and HDPE projectiles appears to be between 22.5° and 30° with HDPE possibly favouring the lower end of the range.

In figure 4, the critical value of $v \sin \theta$, ($v \sin \theta$)^c appears to be around 1 km s^{-1} for both projectiles. Once again though, at values below ($v \sin \theta$)^c, the projectiles display opposite trends which may be accounted for by the amount of contact the projectile makes with the target when skipping off the surface. The phenomena accompanying impacts with $v \sin \theta < (v \sin \theta)^c$ is discussed in section 4.2.

4.1.2. Comparison of crater dimensions with power law predictions.

In figures 5 and 6, the power law predictions of the crater depths p^{pred} and transverse diameters d_c^{pred} (using equation (2)) are plotted against the observed values p^{expt} and d_t^{expt} . Note that, here, the dimensions are normalized to the projectile diameter. Also plotted in the figures are the lines $p^{\text{pred}} = p^{\text{expt}}$ and $d_c^{\text{pred}} = d_t^{\text{expt}}$ respectively. These show reasonable agreement between the prediction and experiment especially at larger values of the crater dimensions.

In addition, the ratios of the power law predictions of the crater depths and diameters to the observed values are also plotted against $v \sin \theta$ in figures 7 and 8. These show, however, that there is a discernible trend in the correlation with respect to $v \sin \theta$.

The value of $v \sin \theta$ above which reasonable agreement occurs for both aluminium and HDPE projectiles appears to be 1 km s^{-1} , for both the depths and diameters, which coincides with the value determined for $(v \sin \theta)^c$ from the circularity in the previous section.

In figure 7, it appears that below $(v \sin \theta)^c$ the trends differ once again for aluminium and HDPE projectiles. The observed crater depths are greater than predicted for aluminium projectiles and vice versa for HDPE. This relative difference in the trends may once again be attributed to the difference in density of the projectiles ($\rho^{\text{HDPE}} = 0.969 \text{ g cm}^{-3}$, $\rho^{\text{Al}} = 2.71 \text{ g cm}^{-3}$) relative to the target ($\rho^{\text{graphite}} = 1.83 \text{ g cm}^{-3}$). The greater density of aluminium implies that there is a longer period of contact with the target at the impact point, thus causing more damage. The diameters in figure 8 however do not show these differing trends. In the following section, the phenomena associated with impacts for which values of $v \sin \theta$ are less than $(v \sin \theta)^c$ are discussed.

4.2 Correlation laws for oblique impacts with below the critical normal velocity

In the following subsections, an attempt is made to derive the correlation laws for the crater depths and diameters (at values of $v \sin \theta < (v \sin \theta)^c$) and the fragmentation angle θ^f .

4.2.1 Crater depth and transverse diameter.

In figure 9, power law correlations have been determined between the normalized crater dimensions and the normal component of the velocity for impacts with $v \sin \theta < 1 \text{ km s}^{-1}$. These are shown in equation (4) along with values for the coefficient of determination R^2 , which is a measure of the goodness of the fits ($R^2 = 1$ indicates a perfect fit). As can be seen from the plots, the trends can only be considered as approximate and requires more data to reduce the scatter of the data points.

$$\begin{aligned} \frac{P}{d_p}^{\text{Al}} &= 1.2(v \sin \theta)^{0.48}; R^2 = 0.79, \\ \frac{d_t}{d_p}^{\text{Al}} &= 3(v \sin \theta)^{0.26}; R^2 = 0.34, \\ \frac{P}{d_p}^{\text{HDPE}} &= 0.9(v \sin \theta)^{1.2}; R^2 = 0.95, \\ \frac{d_t}{d_p}^{\text{HDPE}} &= 2.6(v \sin \theta)^{0.74}; R^2 = 0.79. \end{aligned} \quad (4)$$

As expected, the trends in this regime differ from the correlations derived for normal impacts in table 1. There is also a significant difference between the projectile types with the crater dimensions varying less with the normal component of the impact velocity $v \sin \theta$ for aluminium than observed for HDPE.

An insight into the reasons this may be gained by investigating what happens at impact velocities below the hypervelocity regime [12]. At these low velocities, the projectile behaves as a rigid penetrator and hence the crater dimensions are determined by the plastic flow of materials in the colliding bodies. This behaviour continues as the velocity is increased until the hypervelocity regime is reached and impact induced stresses cause the projectile to break up and finally deform and behave as a fluid.

Figure 10 shows two curves of normalized dimension against impact velocity. The solid curve shows the variation expected for impacts by a projectile (e.g. aluminium) much stronger and denser than the target whilst the dashed curve shows the expected variation for a weaker projectile (e.g. HDPE) impacting a stronger target.

For projectiles like aluminium impacting graphite, the normalized dimension increases rapidly with velocity, at low velocities, with the onset of projectile breakup and deformation marked by a peak in the curve followed by a reduction in projectile effectiveness as the velocity increases into the hypervelocity regime. For HDPE on the other hand, the peak is absent with a smoother progression into the hypervelocity regime observed.

Comparing figure 10 with figure 9, it appears that the data points for aluminium are within the cusp preceding the hypervelocity regime in figure 10 where the dimension slowly increases with velocity. For HDPE, on the other hand, this cusp is absent, hence the rapid variation with velocity observed in the data.

4.2.2 Longitudinal diameter.

For those impacts with $v \sin \theta < (v \sin \theta)^c$, the longitudinal diameter d_l is plotted against the longitudinal component of the impact velocity $v \cos \theta$ in figure 11.

From the plots, it appears that for values of $v \cos \theta > 1 \text{ km s}^{-1}$, there is an approximate linear correlation between d_l and $v \cos \theta$ as expected. Fitting a line through the relevant points gives the following equations.

$$\begin{aligned} \frac{d_l}{d_p}^{Al} &= 0.38 v \cos \theta + 2.6; R^2 = 0.67, \\ \frac{d_l}{d_p}^{HDPE} &= 0.17 v \cos \theta + 1.8; R^2 = 0.9. \end{aligned} \quad (5)$$

4.3 Fragmentation angle

Figure 12 shows a typical experimental set-up for the oblique impacts. The witness plate, typically made of aluminium or an aluminium alloy, is positioned downrange of the impact to catch the ricocheting projectile (intact or fragmented) as well as the ejecta of graphite particles from the crater.

In figures 13 - 16 are photographs of target plates and witness plates for a selection of low angle impacts of aluminium and HDPE projectiles. The projectile trajectory is from left to right.

Figures 13 and 14 show the resulting craters from aluminium impacts at an angle of 5° and speeds of 3 km s^{-1} and 6 km s^{-1} respectively. In figure 13(a), the crater is accompanied by a smear downrange of it which can be attributed to the aluminium projectile ricocheting off the surface intact as the witness plate in figure 13(b) indicates. With an impact velocity of 6 km s^{-1} , a secondary crater is observed downrange of the larger primary crater in figure 14(a). This highlights the onset of fragmentation which is confirmed by the two craters (the projectile fragments into two main pieces) in the witness plate shown in figure 14(b).

Increasing the impact angle to 15° in figure 15(a) yields more and smaller secondary craters downrange of the primary crater which can be attributed to increased fragmentation. The witness plate in figure 15(b) shows three relatively larger craters surrounded by smaller indentations. This may be interpreted as the projectile breaking up into three main pieces and numerous fine particles.

Increasing the impact angle further to 22.5° in figure 16(a), a single crater is now observed in the target plate. The witness plate (figure 16(b)) indicates a spray of fine particles is ejected from the crater which will include both projectile and target material. A similar description can be applied to the craters observed from the impacts of HDPE projectiles.

From the discussion at the beginning of this section, the fragmentation angle θ^f at which the projectile no longer ricochets intact from the target surface appears to be somewhere between 5° and 15° . Furthermore, figures 13 and 14 indicate that θ^f is velocity-dependent since the projectile ricochets intact from the surface at a speed of 3 km s^{-1} but appears to fragment into two pieces when traveling at 6 km s^{-1} . In Table 3, these results are summarized along with those from some additional experiments. Also shown are the values of the normal

velocity components for the experiments. These indicate that fragmentation appears to commence at $(v \sin \theta)^f \approx 0.5 \text{ kms}^{-1}$.

Table 3. Target and witness plate descriptions.

Projectile Material	v/kms^{-1}	θ^0	$v \sin \theta/\text{kms}^{-1}$	Target plate craters	Witness plate craters
Aluminium	2.93	5	0.26	Primary + smear	Single
Aluminium	5.84	5	0.51	Primary + secondary	Two
Aluminium	1.06	15	0.27	Irregular primary	Single
Aluminium	3.04	15	0.79	Primary + secondaries	Three large + multiple small
Aluminium	5.94	15	1.54	Single	Multiple small
Aluminium	5.04	22.5	1.93	Single	Multiple small
Aluminium	6.05	22.5	2.31	Single	Multiple small
Aluminium	6.06	30	3.03	Single	Multiple small
HDPE	2.88	5	0.25	Multiple small	Single
HDPE	3.12	15	0.81	Primary + secondaries	Three large + multiple small
HDPE	5.13	22.5	1.96	Single	Multiple small
HDPE	6.08	22.5	2.33	Single	Multiple small

5. Conclusions

In summary, this study into the hypervelocity impact of projectiles into graphite targets has:

- Investigated oblique impacts of HDPE and aluminium projectiles into graphite at a wide range of angles.
- Determined the critical value of the normal component of impact velocity $(v \sin \theta)^c$ below which the projectiles no longer deform hydrodynamically to be $\approx 1 \text{ kms}^{-1}$ for both projectiles. Likewise the fragmentation angle θ^f below which the projectile ricochets off the target surface fully intact was determined to fall between 5° and 15° . Alternatively, $(v \sin \theta)^f$ was determined to be $\approx 0.5 \text{ kms}^{-1}$.
- Developed correlation laws for the crater depths p and transverse diameters d_t with $v \sin \theta$ and for the longitudinal diameter d_l with $v \cos \theta$ (for $v \cos \theta > 1 \text{ kms}^{-1}$).

Acknowledgements

The author would like to acknowledge the valuable help received from Cliff Cheesman, Douglas Day, Nigel Thomas, Sarah Price and Wayne Harrison during the compilation of this report. This work was funded by AWE Plc, Aldermaston, Reading, Berkshire RG7 4PR.

Appendix A.

Experimental data

The experimental data obtained from the impact experiments are presented in tables A1 and A2. The notation below has been applied for the parameters.

Table A1. Experimental data for oblique impacts of aluminium projectiles into graphite.

v/kms^{-1}	θ^0	$v\sin\theta/\text{kms}^{-1}$	$v\cos\theta/\text{kms}^{-1}$	t/mm	d_p/mm	p/d_p	d_r/d_p	d_f/d_p
1.046	5	0.09	1.04	25	2.99	0.4	1.7	3.38
1.131	5	0.1	1.13	25	2.04	0.39	2.2	3.47
2.927	5	0.26	2.92	25	2.04	0.39	0.93	2.94
5.837	5	0.51	5.81	50	2.04	0.59	2.83	5.17
1.059	15	0.27	1.02	25	2.04	0.68	2.43	2.75
3.043	15	0.79	2.94	25	2.04	1.06	3	3.72
5.941	15	1.54	5.74	50	2.04	1.61	4.4	4.75
0.942	22.5	0.36	0.87	25	2.04	0.83	2.16	2.27
2.042	22.5	0.78	1.89	25	2.04	1.08	2.89	3.51
5.042	22.5	1.93	4.66	50	2.04	1.91	5.39	5.15
6.048	22.5	2.31	5.59	50	2.04	2.26	5.69	6.03
1.037	30	0.52	0.9	25	2.04	1.01	2.89	2.71
2.019	30	1.01	1.75	25	2.04	1.25	3.57	3.93
6.061	30	3.03	5.25	50	2.04	2.46	7.6	7.5
1.101	60	0.95	0.55	50	2.04	1.2	3.13	2.96
6.061	60	5.25	3.03	50	2.04	3.04	8.59	8.49

Table A2. Experimental data for oblique impacts of HDPE projectiles into graphite.

v/kms^{-1}	θ^0	$v\sin\theta/\text{kms}^{-1}$	$v\cos\theta/\text{kms}^{-1}$	t/mm	d_p/mm	p/d_p	d_r/d_p	d_f/d_p
1.057	5	0.09	1.05	25	3.15	No visible crater		
2.21	5	0.19	2.2	25	3.15	Irregular multiple craters		
2.878	5	0.25	2.87	25	3.15	Irregular multiple craters		
2.24	10	0.39	6.01	25	3.15	0.17	1.21	4.56
5.98	10	1.04	5.89	25	3.15	0.61	2.19	3.05
0.946	15	0.25	0.91	25	3.15	0.17	0.77	0.31
3.124	15	0.81	3.02	25	3.15	0.63	2.49	2.31
3.28	15	0.85	3.17	10	3.15	0.66	2.14	2.54
6.22	15	1.61	3.17	10	3.15	0.65	2.52	3.06
0.912	22.5	0.35	0.84	25	3.15	0.22	1.22	0.96
1.978	22.5	0.76	1.83	25	3.15	0.78	1.83	2.06
5.127	22.5	1.96	4.74	50	3.15	1.13	3.43	3.59
6.084	22.5	2.33	5.62	50	3.15	1.41	3.71	3.27
0.942	30	0.47	0.82	25	3.15	0.44	2.24	1.7
1.996	30	1	1.73	25	3.15	0.87	2.39	2.13
2.48	30	1.24	2.15	10	3.15	0.91	2.52	2.62
6.059	30	3.03	5.25	50	3.15	1.65	4.57	4.57
4.12	45	2.91	2.91	10	3.15	1.5	4.05	4.3
1.038	60	0.9	0.52	50	3.15	0.71	2.29	2.06
5.94	60	5.14	2.97	50	3.15	2.38	6.73	5.62

References

- [1] Shanbing Y, Gengchen S and Qingming T 1994 *Int. J. Impact Eng* **15** 1 67-77
- [2] Cour-Palais B G 1987 *Int. J. Impact Eng* **5** 221-237
- [3] Taylor E, Kay L and Shrine N 1997 *Adv. Space Res.* **20** 8 1437-1440
- [4] Schultz, P. H., C. A. Eberhardy, C. M. Ernst, M. F. A'Hearn, J. M. Sunshine, and C. M. Lisse 2007, *Icarus* **190**, 295-333
- [5] Schultz, P. H., and D. E. Gault 1990, Proceedings of the Global Catastrophes in *Earth History: An Interdisciplinary Conference on Impacts, Volcanism, and Mass Mortality*, Geological Society of America Special Paper 247, 239-261.
- [6] Latunde-Dada S, Cheesman C, Day D and Price S 2011 *J.Phys. Conf. Series* **286**
- [7] Gault D E and Wedekind J A 1978 *Proc. Lunar Planet. Sci. Conf. 9th* 3843-3875
- [8] Burchell M J and Grey I D S 2001 *Material Science and Engineering* **A303** 1340141
- [9] Christiansen E L, Cykowski E and Ortega J 1993 *Int. J. Impact Eng* **14** 1 157-168
- [10] Partridge W S and Vanfleet H B 1958 *Astrophysical Journal* **128** 416
- [11] Schultz and Crawford 2011 *GSA Special Publication* **477**
- [12] Zukas A J, Nichols T, Swift H F, Greszczuk L B and Curran D R 1982 *Impact Dynamics* (New York: John Wiley and Sons) p215-221